Molecular Vision 2022; 28:178-191 <http://www.molvis.org/molvis/v28/178>
Received 18 February 2022 | Accepted 5 August 2022 | Published 7 August 2022

Hsa-miR-150-5p inhibits Wnt-β-catenin signaling in human corneal epithelial stem cells

Lavanya Kalaimani,[1,4,5] Bharanidharan Devarajan,[2] Venkatesh Prajna Namperumalsamy,[3] Muthukkaruppan Veerappan,[1] Julie T. Daniels,[5] Gowri Priya Chidambaranathan[1,4]

[1]Department of Immunology and Stem Cell Biology, Aravind Medical Research Foundation, Madurai, Tamil Nadu, India; [2]Department of Microbiology and Bioinformatics, Aravind Medical Research Foundation, Madurai, Tamil Nadu, India; [3]Cornea Clinic, Aravind Eye Hospital and Postgraduate Institute of Ophthalmology, Madurai, Tamil Nadu, India; [4]Department of Biotechnology, Aravind Medical Research Foundation -Affiliated to Alagappa University, Karaikudi, Tamil Nadu, India; [5]Institute of Ophthalmology, University College London, London, United Kingdom

Purpose: In our earlier study, we identified hsa-miR-150-5p as a highly expressed miRNA in enriched corneal epithelial stem cells (CESCs). In this study, we aimed to understand the molecular regulatory function of hsa-miR-150-5p in association with the maintenance of stemness in CESCs.

Methods: The target mRNAs of hsa-miR-150-5p were predicted and subjected to pathway analysis to identify targets for functional studies. Primary cultured limbal epithelial cells were transfected with hsa-miR-150-5p mimic, inhibitor, or scrambled sequence using Lipofectamine 3000. The transfected cells were analyzed to determine (i) their colony-forming potential; (ii) the expression levels of stem cell (SC) markers/transcription factors (ABCG2, NANOG, OCT4, KLF4, and ΔNp63), the differentiation marker (Cx43), and the hsa-miR-150-5p predicted targets (JARID2, INHBA, AKT3, and CTNNB1) by qPCR; and (iii) the expression levels of ABCG2, p63α, Cx43, JARID2, AKT3, p-AKT3, β-catenin, and active β-catenin by immunofluorescence staining and/or western blotting.

Results: The ectopic expression level of hsa-miR-150-5p increased the colony-forming potential (8.29% ± 0.47%, $p < 0.001$) with the ability to form holoclone-like colonies compared with the control (1.8% ± 0.47%). The mimic-treated cells had higher expression levels of the SC markers but reduced expression levels of Cx43 and the targets of hsa-miR-150-5p that are involved in the Wnt-β-catenin signaling pathway. The expression levels of β-catenin and active β-catenin in the inhibitor-transfected cells were higher than those in the control cells, and the localized nuclear expression indicated the activation of Wnt signaling.

Conclusions: Our results indicate a regulatory role for hsa-miR-150-5p in the maintenance of CESCs by inhibiting the Wnt signaling pathway.

The cornea is the transparent window of the eye, and its outermost layer, the corneal epithelium, plays an essential role in maintaining corneal transparency [1]. Corneal epithelial stem cells (CESCs) in the basal layer of the limbal epithelium maintain corneal epithelial homeostasis [2]. These adult stem cells are tissue-specific and located in a specialized niche in the limbus. They are normally quiescent and proliferate during wound healing [3] and maintain homeostasis throughout life [4]. Although many reports are available on their properties such as migration [5], angiogenesis [6], differentiation [7], and proliferation [8], resources on the molecular regulation of stemness are limited. A few reports on growth factors [9], transcription factors [10], and miRNAs [11] suggest the possibility of CESC regulation.

MiRNAs are non-coding single-stranded RNAs containing 18–24 nucleotides that are involved in the post-transcriptional regulation of gene expressions [12, 13]. To understand the miRNA profile of CESCs in relation to the maintenance of stemness, we previously performed small RNA sequencing of enriched human CESCs in comparison with differentiated central corneal epithelial cells. CESCs were enriched up to 80% using a two-step enrichment protocol: (i) differential enzymatic treatment to isolate the basal limbal epithelial cells (25% stem cell content [14]), followed by (ii) laser capture microdissection of cells with a nucleus-to-cytoplasm ratio of ≥0.7 (80% stem cell content [15]). Six miRNAs, namely hsa-miR-21-5p, hsa-miR-143-3p, hsa-miR-150-5p, hsa-miR-3168, hsa-miR-1910-5p, and hsa-miR-10a-5p, were identified as highly expressed in CESCs and validated with qPCR analysis. In addition, miRNA

Correspondence to: Gowri Priya Chidambaranathan, Department of Immunology and Stem Cell Biology, Aravind Medical Research Foundation, Madurai, Tamil Nadu- 625020, India; Phone: +91452-4356550- Extension 433/441; FAX: 91-452-2530984; email: gowri@aravind.org

locked nucleic acid in situ hybridization revealed that hsa-miR-150-5p was expressed in clusters of small cells in the limbal basal epithelium, which indicates their association with stem cells [16]. In continuation of our previous work on miRNA profiling, we analyzed the functional role of hsa-miR-150-5p in CESCs in this study.

Hsa-miR-150-5p is known to be involved in various cellular functions in different types of cells. Myocardial remodeling and cardiomyocyte apoptosis were prevented in rat models of ischemia/reperfusion when extracellular vesicles carrying miR-150-5p derived from mesenchymal stem cells were transferred intramyocardially [17]. Hsa-miR-150-5p has also been found to regulate cell cycle progression [18], proliferation [19], differentiation [20], mesenchymal-epithelial transition [21], tumorigenesis [22], and various pathways such as Wnt-β-catenin signaling [23].

The behavior of three-dimensional (3-D) cultured cells is similar to in vivo responses of the cells; hence, 3-D culture systems are considered an excellent in vitro model. The tissue equivalents (TEs) of Real Architecture For 3D Tissue (RAFT) are spatially defined compressed collagen-based 3-D culture systems for producing mimetic epithelial or endothelial tissue equivalents suitable for transplantation and a model for studying cellular interactions [24]. This RAFT culture system is ideal for culturing primary limbal epithelial cells, including CESCs, in their relatively native-like environment for functional analysis [25]. Hence, in this study, to elucidate the regulatory potential of hsa-miR-150-5p in CESCs, the RAFT system was used to culture limbal epithelial cells. Understanding the regulatory mechanism of hsa-miR-150-5p, including the signaling pathways, will be beneficial for developing therapeutic applications based on miRNAs and for expanding autologous CESCs for transplantation in limbal stem cell-deficient (LSCD) patients.

METHODS

Sample: Human donor tissues were handled in accordance with the tenets of the Declaration of Helsinki, and the study was approved by the institutional ethics committee, Aravind Medical Research Foundation (RES2013038BAS), and the Moorfields Eye Hospital/UCL Institute of Ophthalmology Eye Tissue Repository 10/H0106/57-2011ETR10. The enucleated donor globes and limbal rims received after transplantation (donor age, ≤72 years; non-diabetic) were obtained from the Rotary Aravind International Eye Bank (Madurai, India), Moorfields Eye Hospital Lions Eye Bank (London, UK), and Veneto Eye Bank Foundation (Venice, Italy). The donor globes used in the study were observed under a stereo binocular microscope, and those with intact limbus were selected.

Target prediction for hsa-miR-150-5p: The targets of hsa-miR-150-5p were predicted using miRWalk Version 3.0 [26] and mirDIP Version 4.1.1.6 [27]. Targets that were common to both miRWalk and mirDIP were selected to avoid false positives. The selected targets were analyzed using the Kyoto Encyclopedia of Genes and Genomes (KEGG) mapping tool, the Search pathway in the KEGG mapper, and grouped into functional categories. The targets associated with the regulation of stem cells were selected for further analysis.

Two-dimensional limbal epithelial cell culture: Limbal epithelial cells from limbal explants (2 mm) from donor eyes/limbal rims were cultured, as described by Arpitha et al. [28]. Briefly, the explants were placed in a 35-mm cell culture dish (Nunc, Thermo Fisher Scientific, Waltham, MA), with the epithelial side facing up. The explants were covered with a drop of supplemented hormonal epithelial medium (SHEM) and allowed to attach to the dish by incubating at 37°C for approximately 20 min. The medium was composed of DMEM/F12 Glutamax (Invitrogen, Thermo Fisher Scientific), fetal bovine serum (10%, Invitrogen), dimethyl sulfoxide (0.5%, Sigma-Aldrich, St Louis, MO), transferrin (5 µg/ml, Sigma-Aldrich), insulin (5 µg/ml; Invitrogen), hydrocortisone (0.5 µg/ml; Sigma-Aldrich), sodium selenite (5 ng/ml; Sigma-Aldrich), amphotericin B (1.25 µg/ml; Invitrogen), gentamicin (50 µg/ml; Invitrogen), and epidermal growth factor (5 ng/ml; Invitrogen). After attachment, the explants were cultured in SHEM at 37°C and 5% CO_2. The medium was changed on alternate days until it reached 70% to 80% confluency.

3-D limbal epithelial cell culture: The limbal epithelial cells were isolated, as described by Arpitha et al. [29]. Briefly, the limbal ring was treated with dispase II (2 mg/ml) for 45 min at 37°C, followed by trypsin (0.25%) treatment for 30 min to obtain individual epithelial cells. In the 3-D culture, the isolated limbal epithelial cells were grown on RAFT-TEs containing corneal stromal stem cells (CSSCs).

For culturing the CSSCs, the limbus, along with the anterior stroma, was dissected (approximately 100 µm deep), leaving a small portion of sclera on one side and the cornea on the other side. The limbal stroma was cut into small pieces and incubated in a collagenase solution (Collagenase-L 0.5 mg/ml) at 37°C overnight. After centrifugation, the pellet from the digested solution was resuspended in 3 ml of CSSC medium [30]. The cells were then incubated at 37°C in 5% CO_2 in a fibronectin-coated T25 flask. On the next day, the cells adhering to the flask were washed with 1× Dulbecco's phosphate-buffered saline (Life Technologies, Paisley, UK)

and replaced with fresh CSSC medium. On the second day, the CSSCs were selectively trypsinized with 0.05% trypsin-0.02% EDTA (Invitrogen), transferred to a fresh fibronectin-coated T75 flask, and cultured at 37°C in 5% CO_2, with medium replacement on alternate days. When the cells reached 60%–70% confluence, they were subcultured at a seeding density of 3000 cells/cm^2 in a fresh flask. The cells at passage 4 were used for the preparation of the RAFT.

RAFT TEs were prepared using the method of Levis and Daniels [31], with modifications. Briefly, the collagen solution was prepared by mixing eight parts of AteloCell native collagen (bovine dermis, 3 mg/mL, pH 3.0; Collagen Acidic Solution I-AC, Koken, Tokyo, Japan) with one part of 10× minimum essential medium from a RAFT reagent kit (Lonza, Basel, Switzerland). A neutralizing solution (5 M sodium hydroxide) was added dropwise to achieve a pH between 7.2 and 7.4. The solution was spun at 162 ×g for 3 min to allow the dispersion of any small bubbles. The CSSCs were resuspended in one part of the CSSC medium (30,000 cells/RAFT) and added to the neutralized collagen. The solution was placed in ice to prevent gelling during the preparation process. A volume of 625 µl of freshly prepared collagen solution with CSSCs was transferred into the individual wells of a 24-well plate (Greiner, Stonehouse, UK) and heated to 37°C for 30 min to aid fibrillogenesis to form the hydrogel. Once the collagen gels were formed, RAFT absorbers for 24-well plates (hydrophilic porous absorbers; Lonza) were applied to the surface of the hydrogels for 30 min. Then, the absorbers were gently removed, and fresh CSSC medium was added to the RAFT TEs and stored at 37°C. The limbal epithelial cells were seeded at a density of 2.5 × 10^3 cells/RAFT in a 24-well plate and cultured in a SHEM medium at 37°C and 5% CO_2. The cells were cultured until they reached 70% to 80% confluency with medium on alternate days.

miRNA transfection: To elucidate the functional association of hsa-miR-150-5p with the maintenance of stemness, human primary limbal explant cultures (70%–80% confluent) grown in both two-dimensional (2-D) and 3-D culture systems were transfected with 25 nM of hsa-miR-150-5p mimic (miScript miRNA Mimic, Qiagen, Hilden, Germany) or inhibitor (miScript miRNA Inhibitor, Qiagen) or control scrambled sequence (AllStars Negative Control siRNA, Qiagen) using the Lipofectamine 3000 transfection reagent (Thermo Fisher Scientific), following the manufacturer's instructions. Transfection was performed for 4 h at 37°C in a 5% CO_2 incubator. After 48 h of transfection, the cells were harvested for the following experiments: (i) colony-forming assay, (ii) RNA isolation for qPCR analysis, (iii) immunofluorescence staining, and (iv) protein isolation for western blotting. The experiments were replicated three times with three biological samples (n = 3).

Colony-forming assay: The hsa-miR-150-5p mimic or inhibitor or scrambled control transfected cells were seeded on a mitomycin C (4 µg/ml; Sigma-Aldrich)-treated NIH 3T3 mouse fibroblast feeder layer in a 60-mm dish at a seeding density of 500 cells per plate. The cells were cultured in SHEM. After 12 days of culture, the feeder layer was removed with 0.02% EDTA solution (Sigma-Aldrich), and the colonies in the dish were fixed with 4% paraformaldehyde (Sigma-Aldrich) for 15 min, followed by staining with 1% rhodamine B (Roche, Basel, Switzerland) for 30 min. The colonies were imaged (D750 camera, Nikon, Japan) after washing three times with sterile distilled water. The colony-forming efficiency was calculated by dividing the number of colonies formed by the number of cells seeded ×100. Colonies with an area larger than 10 mm^2 were defined as holoclone-like with respect to their size and morphology [32].

qPCR: Total RNA was isolated from the three groups: (i) mimic, (ii) inhibitor, and (iii) scrambled treated (transfection control) using an RNeasy mini kit (Qiagen). Reverse transcription was performed using a high-capacity cDNA reverse transcription kit (Thermo Fisher Scientific) in accordance with the manufacturer's instruction. Then, qPCR amplification was performed using KAPA SYBR FAST qPCR Master Mix (2×; Sigma-Aldrich) for 40 cycles (denaturation: 10 s at 95°C; annealing: 20 s at 58°C, and extension: 30 s at 72°C) preceded by initial activation for 3 min at 95°C and followed by final extension for 7 min at 72°C. Glyceraldehyde 3-phosphate dehydrogenase (*GAPDH*) was used as reference mRNA. The experiment was repeated three times using the limbal epithelial cells grown in the 2-D culture system, and data were presented as mean ± SD of the expression value. The primers used for the qPCR are listed in Appendix 1.

Immunofluorescence staining: After 48 h of transfection, the cells grown in the 2-D culture system were trypsinized with TrypLE Express (Gibco-Thermo Fisher Scientific) and cytocentrifuged (11 ×g; 3 min) on the slides (2.5 × 10^4 cells/slide). This trypsinization step was skipped for cells grown in the RAFT system; instead, they were fixed directly on the RAFT and immunostained. The cells were fixed with 4% paraformaldehyde for 20 min and permeabilized with 0.5% Triton X-100 for 10 min at room temperature. After permeabilization, the cells were blocked for 60 min in 5% goat serum (Sigma-Aldrich) and incubated with a primary antibody in 2% goat serum in a wet chamber at 4°C overnight (see Appendix 2 for a list of primary antibodies used for immunostaining). The cells were then incubated with an appropriate secondary antibody (1:500) conjugated with

fluorophore in PBS for 60 min at room temperature. Between each step, the slides were washed three times with PBS. After staining, the cells were mounted using a Vectashield mounting medium with DAPI (Vector Laboratories Ltd, Peterborough, UK) and sealed with a coverslip. The primary antibodies in the optimized concentration were used for the staining, and the corresponding isotype controls were used as negative controls. The experiment was replicated three times using three biological samples (n = 3).

Western blotting: The transfected cells were washed with ice-cold PBS (Gibco, Thermo Fisher Scientific) and then lysed with a radioimmunoprecipitation assay lysis and extraction buffer (Thermo Fisher Scientific) and a Halt protease inhibitor cocktail (Thermo Fisher Scientific). The protein concentration was estimated using a bicinchoninic acid protein assay kit (Pierce, Thermo Fisher Scientific). Equal concentrations of protein from each sample (20 µg) were mixed into a lithium dodecyl sulfate sample-loading buffer (Thermo Fisher Scientific), boiled for 10 min, and separated using 10% Bis-tris gel (NuPAGE, Thermo Fisher Scientific) under reducing conditions.

The separated proteins were then electrotransferred to a polyvinylidene fluoride membrane (Invitrolon, Thermo Fisher Scientific). The membrane was blocked with 5% skimmed milk in Tris-buffered saline containing 0.1% Tween-20 (TBST) and incubated at 4°C overnight with a primary antibody (see Appendix 3 for a list of primary antibodies used for western blotting). The membranes were washed three times with TBST and incubated with the appropriate horseradish peroxidase-conjugated secondary antibody at room temperature for 1 h (Cell Signaling Technology, Inc., Danvers, MA). After three washes, the protein bands were detected using an enhanced chemiluminescence reagent (Millipore, Billerica, MA). All membranes were stripped and reprobed with anti-GAPDH antibody, which was used as loading control and normalizing reference. The experiment was repeated three times using the limbal epithelial cells grown both in the 2-D and 3-D culture systems, and the data were presented as mean ± SD.

Statistical analysis: The statistical software Stata 14.0 (StataCorp LLC, College Station, TX) was used for the statistical analysis. All the experiments were performed in triplicate, and the data obtained were presented as mean ± SD. For data following a Gaussian distribution, an independent *t* test (parametric) was performed to compare the two experimental groups, and the Mann-Whitney *U* test (non-parametric) was used for data that followed a non-Gaussian distribution based on the Shapiro-Wilk normality test. A p value < 0.05 was considered statistically significant.

RESULTS

Predicted target genes of hsa-miR-150-5p: For hsa-miR-150-5p, miRWalk and mirDIP identified 2219 and 1220 target genes, respectively. A total of 315 common target genes were submitted to the KEGG mapper, and the putative target genes were grouped into 229 KEGG pathways. The pathways included MAPK, Wnt, PI3K-AKT, and a signaling pathway associated with the pluripotency of stem cells. AKT serine/threonine kinase 3 (AKT3), Beta catenin 1 (CTNNB1), inhibin subunit beta A (INHBA), and Jumonji and AT-rich interaction domain containing 2 (JARID2) were the four targets involved in the signaling pathways regulating the pluripotency of stem cells, and they were selected for further analysis. The results of the KEGG pathway analysis [33] showing the selected target genes of hsa-miR-150-5p are presented in Appendix 4.

Downregulation of the predicted targets of hsa-miR-150-5p: After transfection, the hsa-miR-150-5p mimic transfected cells showed increased expression levels of hsa-miR-150-5p, and the inhibitor transfected cells showed reduced expression levels compared with the control cells ($p < 0.0001$; Figure 1A). The expression levels of the four selected target mRNAs of hsa-miR-150-5p, namely (i) *CTNNB1*, (ii) *JARID2*, (iii) *INHBA*, and (iv) *AKT3*, were downregulated ($p < 0.0001$) in the mimic-transfected cells compared with the control cells. However, in the inhibitor-transfected cells, their expression levels were upregulated significantly ($p < 0.0001$; Figure 1B). Similarly, at the protein level, the mimic-transfected cells had reduced expression levels of β-catenin, JARID2, and AKT3 compared with the control cells and vice versa in the inhibitor-transfected cells ($p < 0.05$; Figure 2) by western blotting and immunostaining (Figure 3). The number of cells with high nuclear expression levels of β-catenin was increased in the inhibitor-transfected group (37.68% ± 6.24%, $p < 0.05$) but decreased in the mimic-transfected group (4.07% ± 1.4%, $p < 0.05$) compared with the control group (18.54% ± 5.45%; Figure 3).

Hsa-miR-150-5p upregulated the expression levels of the stem cell markers and downregulated that of the differentiation marker: At the mRNA level, the mimic-transfected cells showed significantly higher expression levels of the stem cell markers compared with the control cells ($p < 0.001$): (i) the universal stem cell marker, *ABCG2*; (ii) limbal stem cell marker, *ΔNp63*; and (iii) embryonic stem cell markers, namely *OCT4*, *NANOG*, and *KLF4* (Figure 1C). By contrast, the expression level of the differentiation marker connexin 43 (*Cx43*) was reduced in the mimic-transfected cells. On the other hand, in the inhibitor-transfected cells, the expression levels of the stem cell markers were reduced and the *Cx43*

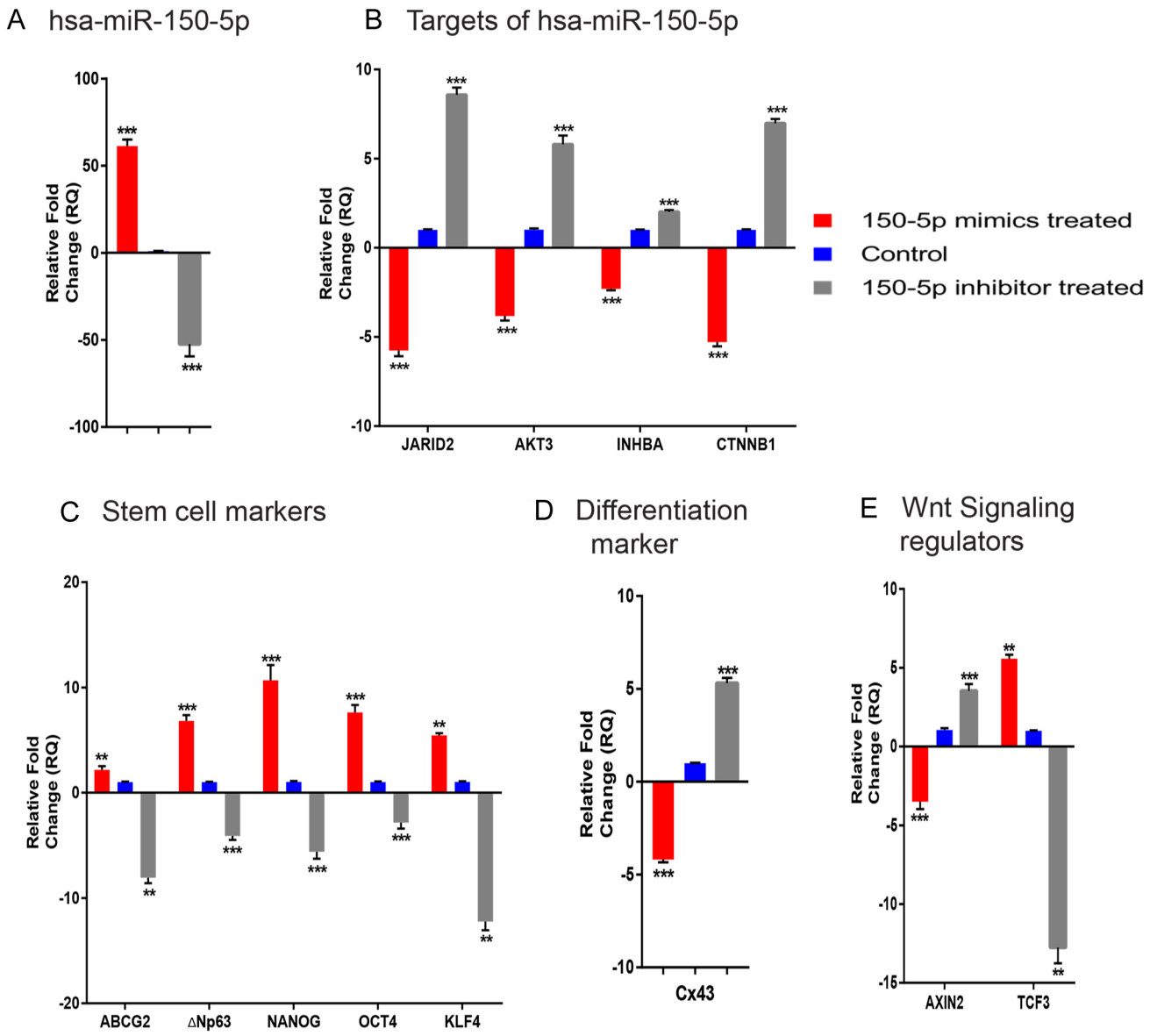

Figure 1. mRNA expression profile of hsa-miR-150-5p-transfected cells. The figure depicts the expression profiles of **A**: hsa-miR-150-5p, **B**: its predicted targets, **C**: the stem cell markers, **D**: the differentiation marker, and **E**: the Wnt signaling regulators upon transfection with the hsa-miR-150-5p mimic and inhibitor. The relative mRNA/miRNA expressions in the mimic- and inhibitor-transfected cells were quantified in comparison with those of the controls by using qPCR with SYBR Green chemistry. Each sample (n = 3) was run in triplicate. The data were expressed as mean ± SD, and the relative fold change of expression (RQ) was calculated using the $2^{-\Delta\Delta CT}$ method after normalization with *GAPDH* (reference gene)/RNU6B (reference microRNA). **p < 0.001; ***p < 0.0001.

expression level was increased compared with the control cells (p < 0.0001; Figures 1D and 3).

Confocal analysis of the mimic-transfected cells revealed a significant increase in the number of cells (42.38 ± 13.57, p < 0.05), which were double-positive for ABCG2 and p63α, compared with the controls (16.25 ± 2.55), and the reverse was true for the inhibitor-transfected cells (2.75 ± 2.47, p < 0.05; Figure 3).

The expression levels of the stem cell and differentiation markers in the transfected cells by western blot analysis were concordant with the mRNA expression pattern of the transfected cells. The expression levels of ABCG2 and ΔNp63α

were upregulated ($p < 0.05$) and the Cx43 expression level was downregulated ($p < 0.05$) in the mimic transfected cells (Figure 2).

To confirm the presence of stem cells in the transfected cultures, a colony-forming assay was performed. The mimic-treated cells showed an increased percentage of colony-forming efficiency (8.28 ± 0.33, $p = 0.0003$) compared with the controls (1.8 ± 0.15) and inhibitor-treated cells (0.71 ± 0.10, $p = 0.001$; Table 1). In addition, the percentage of holoclone-like colonies significantly increased (3.80 ± 0.84, $p < 0.05$) compared with that of the controls (1.11 ± 1.11), whereas the inhibitor-treated cells produced no such larger colony (Figure 4). Thus, the higher expression level of hsa-miR-150-5p in the transfected cells increased the colony-forming efficiency and supported holoclone-like colony formation.

Effect of hsa-miR-150-5p on Wnt signaling: In concordance with the reduced expression level of β-catenin, the direct target of hsa-miR-150-5p, the mRNA expression level of *AXIN2* was also reduced (−3.50 ± 0.46, $p < 0.0001$) in the mimic-transfected cells compared with the controls, indicating the downregulation of active Wnt signaling. However, in the inhibitor-transfected cells, the *AXIN2* expression level was increased 3.53- ± 0.43-fold ($p < 0.0001$). By contrast, the Wnt signaling transcriptional repressor *TCF3* mRNA expression level was upregulated in the mimic-transfected cells and downregulated in the inhibitor-transfected cells ($p < 0.001$; Figure 1E). In the western blotting and immunostaining, the expressions of the Wnt signaling regulators at the protein level showed expression patterns similar to those of the mRNA expressions in the transfected cells. The expression levels of p-AKT3 (negative regulator of GSK3β) and AXIN2 were reduced in the mimic-transfected cells but increased in the inhibitor-transfected cells compared with the controls ($p < 0.05$; Figure 2). Immunostaining revealed that the cells with nuclear positivity for active β-catenin expression were higher in number (86.69% ± 3.57%, $p < 0.001$; Figure 3), and the expression level of active β-catenin was upregulated 1.51- ± 0.28-fold ($p < 0.05$) in the inhibitor-transfected cells compared with the controls (29.21% ± 7.88%) by western blot analysis ($p < 0.05$; Figure 2). By contrast, in the mimic-transfected cells,

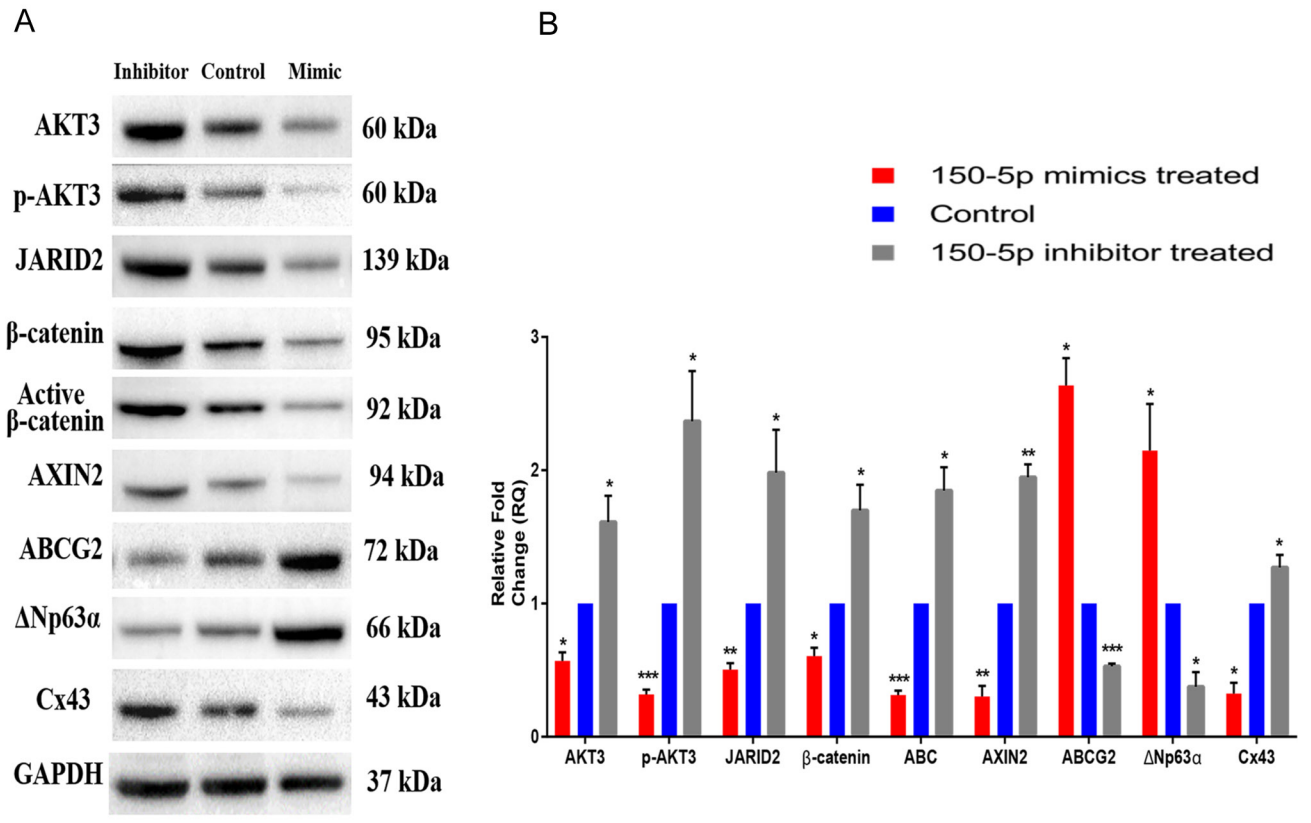

Figure 2. Protein expression profile of the hsa-miR-150-5p-transfected cells grown in the two-dimensional culture system. **A**: The representative western blots of the proteins of interest (AKT3, p-AKT3, JARID2, β-catenin, active β-catenin [ABC], AXIN2, ABCG2, ΔNp63□, and Cx43) in the three groups (hsa-miR-150-5p mimic, inhibitor, and control, n = 3) are shown. GAPDH was used as a normalizing reference and loading control. **B**: The relative expression profiles of the proteins were quantified by western blotting. *$p < 0.05$; **$p < 0.001$; ***$p < 0.0001$.

Table 1. Colony forming assay data.

Observed parameters	miR-150–5p mimic treated	miR-150–5p inhibitor treated	Transfection Control
Total No. of colonies	41.44±1.65	3.55±0.52	9±0.78
Colony forming efficiency (%)	8.28±0.33, p=0.0003	0.71±0.10, p=0.001	1.8±0.15
Holoclone like colonies (%)	3.80±0.84, p=0.0224	0	1.11±1.11

the expression level of active β-catenin was downregulated (0.48 ± 0.15, $p < 0.005$), and the number of cells with nuclear positivity was also reduced (6.44% ± 4.25%, $p < 0.05$). The nuclear localization of active β-catenin is an indication of Wnt signaling activation in the cells.

Effect of hsa-miR-150-5p on CESCs cultured in the RAFT system: The CESCs grown in the RAFT TEs upon transfection with mimic showed reduced expression levels of (i) the hsa-miR-150-5p targets (β-catenin, AKT3, and JARID2), (ii) differentiation marker (Cx43), and (iii) Wnt signaling regulators (AXIN2, active β-catenin, and p-AKT3). However, the expression levels of the stem cell markers ABCG2 and ΔNp63α were increased in the mimic-transfected cells compared with the controls ($p < 0.05$; Figure 5). These results were confirmed by the immunostaining data. In the mimic-transfected cells, β-catenin and active β-catenin positivity was confined to the membrane and cytoplasm, but in the inhibitor-transfected cells, in addition to the membrane and cytoplasm, positivity was observed in the nucleus, indicating nuclear translocation (Figure 6).

DISCUSSION

MicroRNAs have emerged as important regulators of stem cells through the modulation of various signaling pathways [34] and by increasing the expression levels of specific transcription factors [35]. Hsa-miR-150-5p was reported to inhibit cell proliferation and colony formation in glioma through direct targeting of β-catenin [36], a crucial signaling transducer of Wnt-β-catenin signaling [37]. In non-small-cell lung cancer, miR-150-5p suppressed sphere-forming ability and significantly inhibited tumorigenesis by direct targeting of the high mobility group AT-hook 2 (HMGA2) and β-catenin [22]. Although the therapeutic potential of hsa-miR-150-5p and its association with various cancer stem cells are well established, the regulatory role of this miRNA in adult tissue resident stem cells remains elusive.

Reports are available on the miRNA profiling of total human limbal epithelium (≈5% CESCs) and basal limbal epithelium (≈25% CESCs) [38, 39], which represents a heterogenic population of cells. To elucidate the miRNA regulation

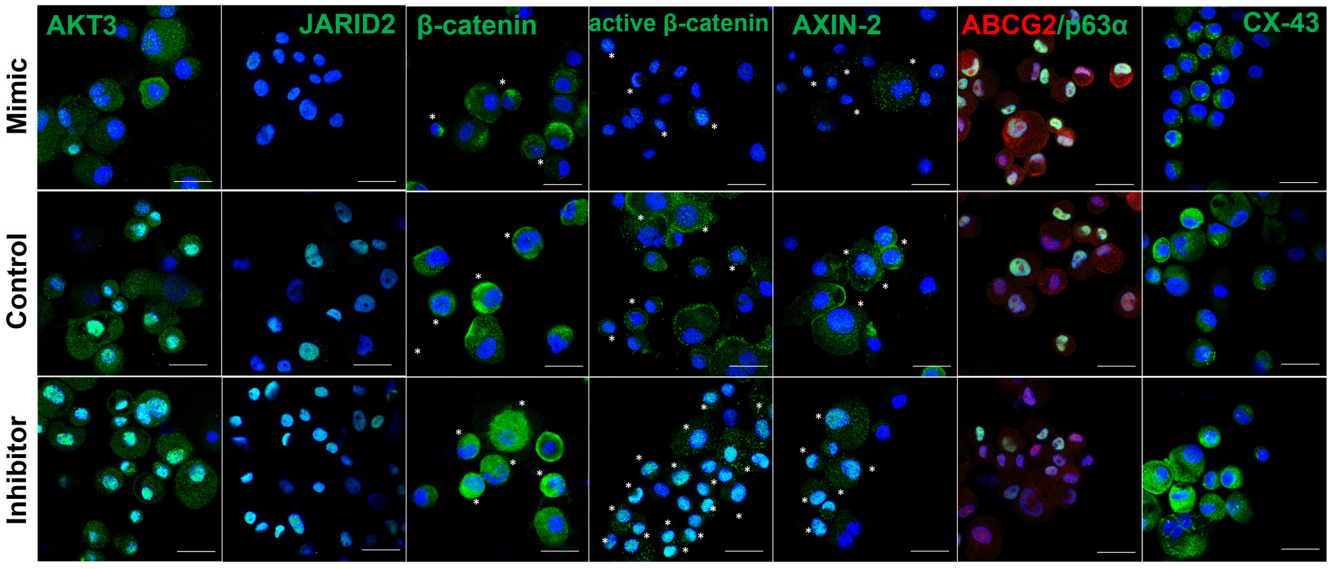

Figure 3. Localization of protein expression in hsa-miR-150-5p-transfected cells. The figures present the representative confocal images of transfected limbal epithelial cells immunostained for AKT3, JARID2, β-catenin, active β-catenin, AXIN2, ABCG2, p63□, and Cx43. Nuclei were represented in blue and protein expression in green or red. The cells with nuclear positivity were marked with asterisks in the Wnt signaling regulators (β-catenin, active β-catenin, and AXIN2). Nuclear localization of active β-catenin is the indication of active Wnt signaling. Scale bar: 50 µm.

of CESCs, it is essential to enrich them, particularly when no marker-based method is available for their isolation. In our previous study, by using an enriched (80%) population of CESCs, small RNA sequencing revealed that hsa-miR-150-5p is highly expressed in these stem cells [16]. To understand the regulatory role of hsa-miR-150-5p in CESCs, miRNA transfection studies were performed on primary limbal explant cultures. The ectopic expression level of hsa-miR-150-5p increased the colony-forming efficiency of the cultured limbal epithelial cells with the ability to form holoclone-like colonies based on size and morphology. In addition, the mimic-transfected cells showed increased expression levels of the stem cell markers and decreased expression level of the differentiation marker. Thus, hsa-miR-150-5p was demonstrated to play a regulatory role in CESCs.

Wnt signaling is known to be involved in both the maintenance and differentiation of stem cells, and its function varies according to cell type, culture condition, and signaling activation level [40-43]. The role of Wnt-β-catenin signaling in limbal epithelial cells has been controversial. Inhibition of Wnt signaling in limbal explant cultures increased the expression levels of stem cell markers (ABCG2 and p63α) and the colony-forming efficiency [42]. By contrast, in the suspension culture of isolated limbal epithelial cells, inhibition of Wnt signaling decreased the colony-forming efficiency and the number of cells expressing high levels of p63α in cultured limbal colonies [44].

In this study, mimic transfection resulted in the downregulation of the Wnt signaling regulators and the three hsa-miR-150-5p-predicted Wnt-β-catenin signaling-specific targets, namely β-catenin, AKT3, and JARID2, both at the mRNA and protein levels. β-catenin, a known direct target of miR-150-5p [22, 36, 45], translocates into the nucleus and interacts with members of the T-cell factor/lymphoid enhancing factor (TCF/LEF) transcription factors, thereby activating the transcription of Wnt-dependent genes [46]. AKT3 is another reported direct target of miR-150-5p [47, 48] and is known to stabilize the Wnt/β-catenin signaling pathway [49]. AKT3 mediates the phosphorylation of β-catenin at Ser552, and this causes β-catenin to dissociate from cell-cell contacts and bind to 14-3-3zeta protein. This interaction leads to enhanced transcriptional activity and stabilization of β-catenin in both the cytosol and nucleus [50, 51]. Phosphorylation of GSK3β by AKT3 leads to the inactivation of GSK3β, which is a negative regulator of Wnt-β-catenin signaling [52]. Thus, AKT3 prevents GSK3β from phosphorylating β-catenin and enhances the stabilization of β-catenin [53, 54]. Hence, the downregulation of AKT3 leads to the inhibition of Wnt-β-catenin signaling through the downregulation of β-catenin, induced by GSK3β. Like various signaling pathways in mammals, Wnt signaling is also negatively regulated by various secreted antagonists such as secreted frizzled-related proteins (SFRPs), WNT inhibitory protein (WIF), and Dickkopf (DKK) family of proteins [55]. SFRPs contain a frizzled (FZD)-like cysteine-rich domain (CRD) that binds competitively to WNT ligands and prevents the interaction between WNTs and FZD receptors, thereby downregulating Wnt signaling. SFRP1 is a direct target of JARID2, and in the cells where JARID2 expression was

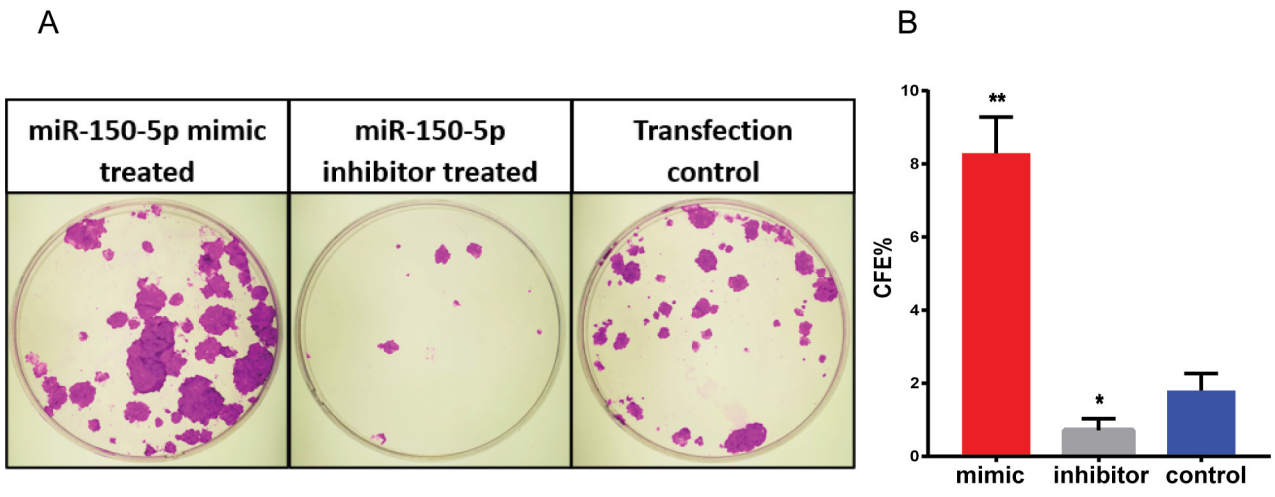

Figure 4. Colony-forming potential of hsa-miR-150-5p-transfected cells. **A**: Representative rhodamine B-stained limbal epithelial cell colonies detected after 12 days of culture in the three groups: hsa-miR-150-5p mimic-, inhibitor-, and control-transfected cells. **B**: The bar graph represents the colony-forming efficiency of the cells in the three groups. *p < 0.05; **p < 0.001.

depleted, Wnt signaling activation was evident [56]. Thus, from this observation, it is clear that JARID2 repressed the expression of the Wnt antagonist SFRP1, thus facilitating the activation of Wnt signaling through Wnt ligand binding.

On the basis of the abovementioned observations, we hypothesized the probable mechanism of action of hsa-miR-150-5p on Wnt-β-catenin signaling, as summarized in Figure 7. Hsa-miR-150-5p prevented the activation of Wnt signaling by downregulating the expression levels of its targets: (i) JARID2, which facilitates Wnt signaling by repressing the expression of the Wnt antagonist SFRP1 and preventing it from binding to FZD receptors; (ii) AKT3, which enhances Wnt signaling by inhibiting GSK3β expression, thereby preventing β-catenin phosphorylation and subsequent degradation; and (iii) β-catenin, which activates Wnt signaling through nuclear localization and induces the expressions of Wnt target genes, including *AXIN2*. Further studies are essential to understand the mechanism by which the expression levels of the transcription factors (OCT4, SOX2, NANOG, KLF4, and p63) are upregulated by hsa-miR-150-5p and the potential role of this miRNA in the direct lineage-specific reprogramming of differentiated corneal epithelial cells to CESCs.

This study demonstrates the potential of hsa-miR-150-5p to inhibit Wnt signaling in primary limbal epithelial cells through the downregulation of the expression levels of the key proteins involved in the pathway. The association of hsa-miR-150-5p in the negative regulation of Wnt signaling in CESCs suggests a cell type-specific function of Wnt signaling within the same niche, as this signaling pathway supports limbal epithelial cell expansion in vitro [44]. Comparative transcriptome profiling and elucidation of the Wnt signaling activity in native CESCs, TACs, and melanocytes will be an intriguing study to explain the varying roles of Wnt signaling

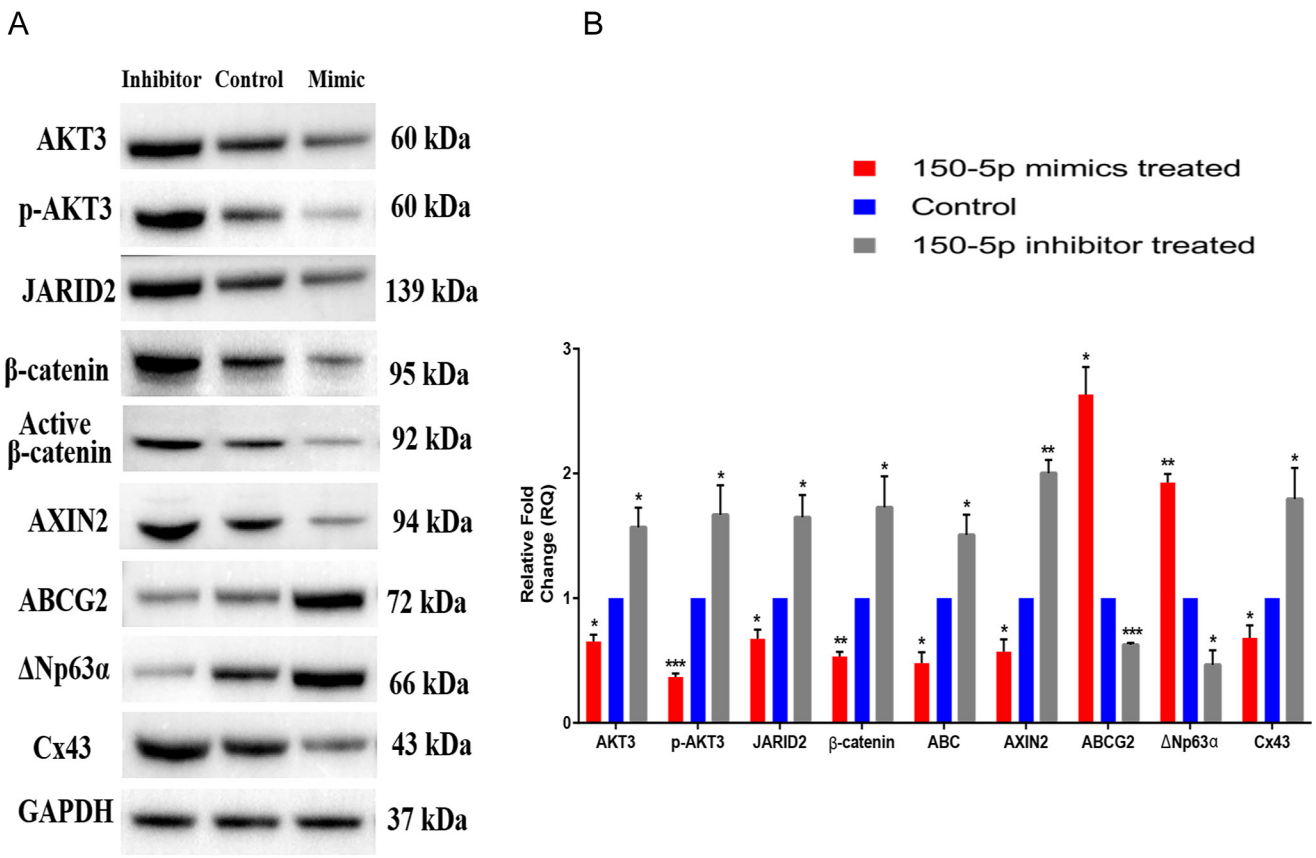

Figure 5. Protein expression profile of hsa-miR-150-5p-transfected cells grown in a Real Architecture For 3D Tissue (RAFT) culture system. **A**: Representative western blots of the proteins of interest (AKT3, p-AKT3, JARID2, β-catenin, active β-catenin, AXIN2, ABCG2, ΔNp63□, and Cx43) in the three groups: hsa-miR-150-5p mimic-, inhibitor-, and control-transfected RAFT cultured cells (n = 3). GAPDH was used as a normalizing reference and loading control. **B**: The relative expression profiles of the proteins were quantified using western blotting. *p < 0.05; **p < 0.001; ***p < 0.0001.

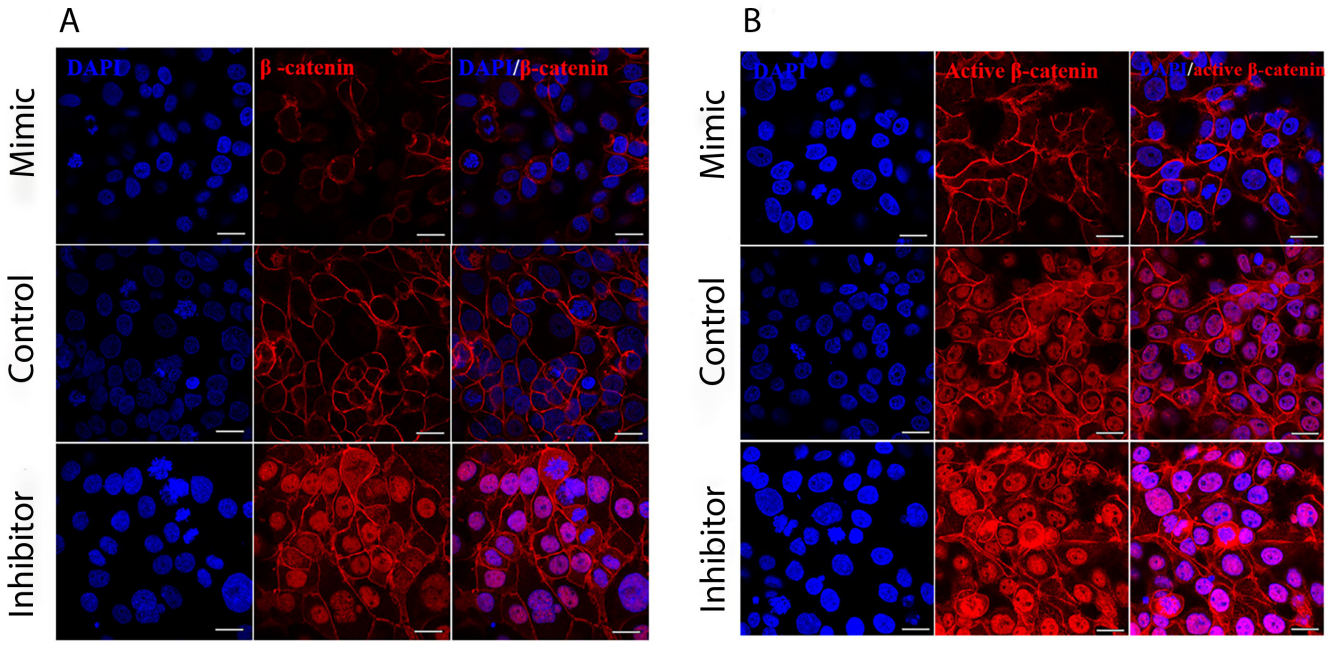

Figure 6. Localization of β-catenin and active β-catenin expressions in hsa-miR-150-5p-transfected cells in Real Architecture For 3D Tissue (RAFT). Shown are representative confocal images of the transfected CESC primary culture cells grown in RAFT TEs immunostained for **A**: β-catenin and **B**: active- β-catenin. Nuclei were represented in blue and protein expression in red. Compared with the control- and mimic-transfected cells, the expression levels of β-catenin and active β-catenin were higher in the inhibitor-transfected cells with nuclear translocation. Nuclear localization of active β-catenin indicates active Wnt signaling. Scale bar: 50 µm.

in different cell types that are present in close proximity. In addition to the effect of hsa-miR-150-5p, elucidating the cumulative effect of other miRNAs that are highly expressed in CESCs [16] is essential for understanding their role in the maintenance of stemness and thus enabling their usage in the development of miRNA-based treatment options for the patients with LSCD.

APPENDIX 1. LIST OF PRIMERS USED IN QPCR.

To access the data, click or select the words "Appendix 1." Fwd- forward; Rev- reverse

APPENDIX 2. LIST OF PRIMARY ANTIBODIES USED FOR IMMUNOSTAINING.

To access the data, click or select the words "Appendix 2."

APPENDIX 3. LIST OF PRIMARY ANTIBODIES USED FOR WESTERN BLOTTING.

To access the data, click or select the words "Appendix 3."

APPENDIX 4. PATHWAY ANALYSIS OF HSA-MIR-150-5P PREDICTED TARGETS.

To access the data, click or select the words "Appendix 4." The figure represents the KEGG pathway analysis of hsa-miR-150-5p predicted targets associated with the pathways regulating pluripotency of stem cells. The targets of hsa-miR-150-5p are represented in red box.

ACKNOWLEDGMENTS

The authors thank Council of Scientific & Industrial Research (CSIR), India for Senior Research Fellowship (09/931(0007)/2018-EMR-I) and Commonwealth Scholarship Commission UK for Commonwealth Split-site scholarship (INCN-2018–72) to Lavanya Kalaimani. Declarations: The authors have no relevant financial or non-financial interests to disclose. Approval was obtained from Institutional Ethics Committee, Aravind Medical Research Foundation (RES2013038BAS) and the Moorfields Eye Hospital / UCL Institute of Ophthalmology Eye Tissue Repository 10/H0106/57–2011ETR10. The procedures used in this study adhere to the tenets of the Declaration of Helsinki. Informed consent was obtained for all donor eyes including the minors from the legally authorized representative - either the

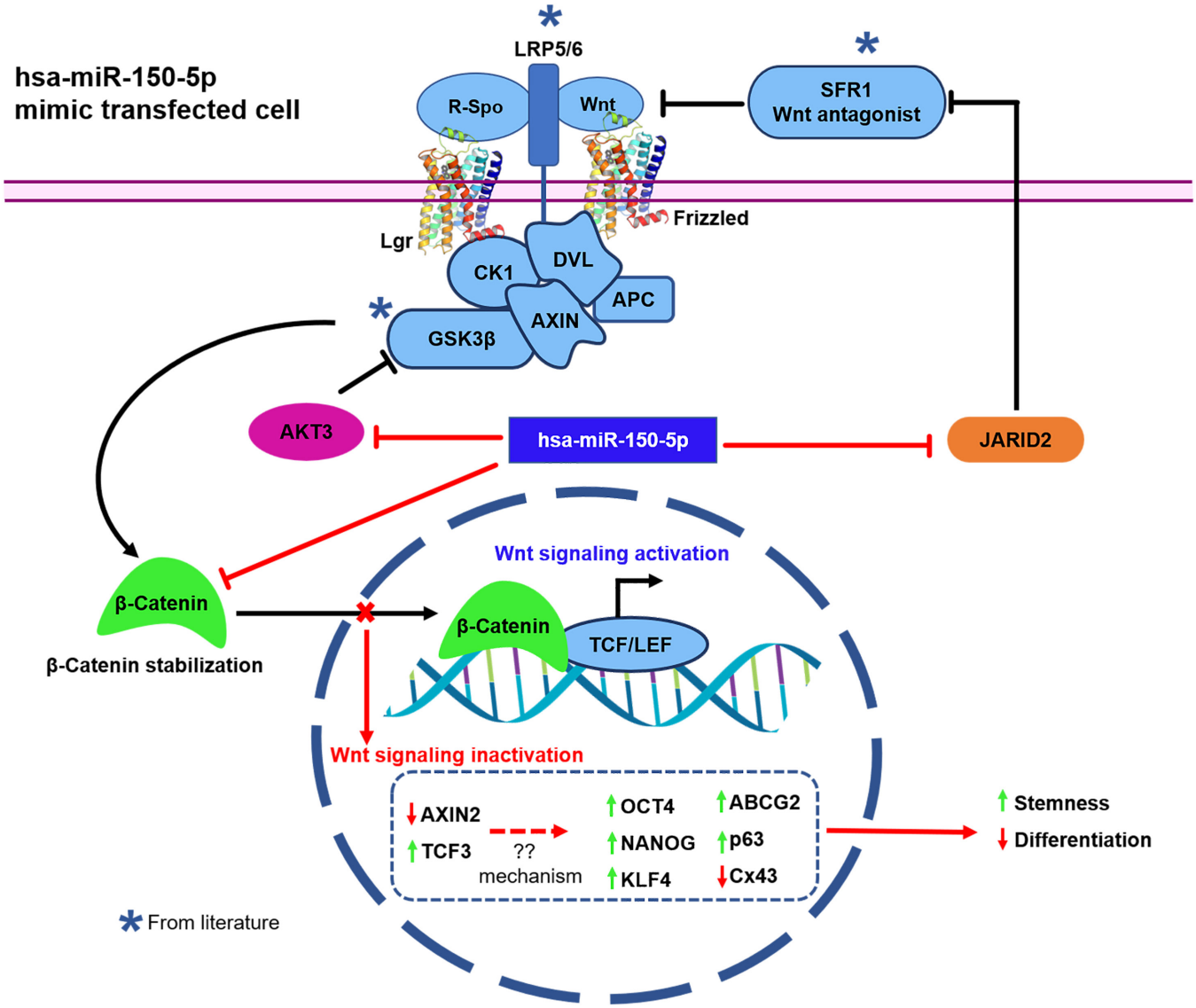

Figure 7. Mechanism of the regulation of Wnt-β-catenin signaling by hsa-miR-150-5p. In the presence of Wnt ligands and Wnt agonists such as R-Spondin (R-Spo), cytoplasmic disheveled (Dvl) is recruited to the membrane receptors, resulting in subsequent phosphorylation and activation of low-density lipoprotein receptor-related protein 5/6 (LRP5/6). These events lead to the titration of the active destruction complex composed of glycogen synthase kinase 3 (GSK3β), casein kinase I (CK1), adenomatosis polyposis coli (APC), and Axin. As a consequence, β-catenin is stabilized and accumulated in the cytoplasm, resulting in the nuclear translocalization of β-catenin, where it activates Wnt signaling through its interaction with the TCF/LEF (T-cell factor/lymphoid-enhancing factor) nuclear complex [57, 58]. Hsa-miR-150-5p prevents the activation of Wnt signaling (red lines) by reducing the expression levels of its targets: (i) β-catenin-Wnt signaling activator (Figure 1B, Figure 2, Figure 3, Figure 5, and Figure 6), (ii) the AKT3 enhancer of β-catenin stabilization through inhibition of GSK3β (Figure 1B, Figure 2, Figure 3, and Figure 5), and (iii) the JARID2 activator of Wnt signaling through the repression of Wnt antagonist-secreted frizzled-related protein 1 (SFRP1; Figure 1B, Figure 2, Figure 3, and Figure 5). This results in a decreased expression level of the Wnt target gene *AXIN2* and an increased expression level of *TCF3*, a Wnt signaling transcriptional repressor.

donor's parents or family through the Eye Banks. Authors' contribution Methodology, data analysis and interpretation, manuscript writing: Lavanya Kalaimani; Study design, data analysis and interpretation: Bharanidharan Devarajan; Data interpretation, proof reading and resources: Venkatesh Prajna Namperumalsamy; Study design, data interpretation, proofreading: Muthukkaruppan Veerappan; Study design, data analysis and interpretation, proofreading: Julie T Daniels; Study design, funding acquisition, data analysis and interpretation, manuscript writing: Gowri Priya Chidambaranathan. The study was funded by Department of Biotechnology, India (No.BT/PR8712/AGR/36/762/2013). Dr. A. Vanniarajan, Scientist, Department of Molecular Genetics, Aravind Medical Research Foundation, Madurai, India, for his guidance in qRT-PCR work. Mr. D. Saravanan, Manager, Rotary Aravind International Eye Bank, Madurai, India for his valuable help in sample collection for the study. Mr. K. Manojkumar, Department of Bioinformatics, Aravind Medical Research Foundation, Madurai, India, for his help in preparing the Figures. Mr. Mohammed Sithiq Uduman, Department of Biostatistics, Aravind Eye Care System, Madurai, India for helping us in the statistics. Dr. R. Kumaragurupari, Chief Librarian, Aravind eye care system for her valuable help in reference formatting and literature collection. Data Availability The data sets generated during and/or analyzed during the current study are available from the corresponding author on reasonable request.

REFERENCES

1. Ouyang H, Xue Y, Lin Y, Zhang X, Xi L, Patel S, Cai H, Luo J, Zhang M, Zhang M, Yang Y, Li G, Li H, Jiang W, Yeh E, Lin J, Pei M, Zhu J, Cao G, Zhang L, Yu B, Chen S, Fu XD, Liu Y, Zhang K. WNT7A and PAX6 define corneal epithelium homeostasis and pathogenesis. Nature 2014; 511:358-61. [PMID: 25030175].

2. Ordonez P, Di Girolamo N. Limbal epithelial stem cells: role of the niche microenvironment. Stem Cells 2012; 30:100-7. [PMID: 22131201].

3. Seyed-Safi AG, Daniels JT. A validated porcine corneal organ culture model to study the limbal response to corneal epithelial injury. Exp Eye Res 2020; 197:108063-[PMID: 32417262].

4. Peng H, Wang J, Yang W, Kaplan N. ID3/LRRK1 is a novel limbal epithelial stem cell regulatory axis. Invest Ophthalmol Vis Sci 2020; 61:2796-.

5. Bonzano C, Canciani B, Olivari S, Papadia M, Bagnis A, Cutolo CA, Bonzano E, Pagani P, Cancedda R, Traverso CE. CFSE: A New Method for Identifying Human Limbal Stem Cells and Following Their Migration in Human Cornea. In Vivo 2019; 33:1851-5. [PMID: 31662512].

6. Notara M, Lentzsch A, Coroneo M, Cursiefen C. The Role of Limbal Epithelial Stem Cells in Regulating Corneal (Lymph)angiogenic Privilege and the Micromilieu of the Limbal Niche following UV Exposure. Stem Cells Int 2018; 2018:8620172-[PMID: 29853920].

7. Sagga N, Kuffová L, Vargesson N, Erskine L, Collinson JM. Limbal epithelial stem cell activity and corneal epithelial cell cycle parameters in adult and aging mice. Stem Cell Res (Amst) 2018; 33:185-98. [PMID: 30439642].

8. Holan V, Trosan P, Krulová M, Zajicova A. Identification of factors regulating differentiation and growth of limbal stem cells for corneal surface regeneration. Acta Ophthalmologica. 2012; 90:249-.

9. Kolli S, Bojic S, Ghareeb AE, Kurzawa-Akanbi M, Figureueiredo FC, Lako M. The Role of Nerve Growth Factor in Maintaining Proliferative Capacity, Colony-Forming Efficiency, and the Limbal Stem Cell Phenotype. Stem Cells 2019; 37:139-49. [PMID: 30599086].

10. Bhattacharya S, Serror L, Nir E, Dhiraj D, Altshuler A, Khreish M, Tiosano B, Hasson P, Panman L, Luxenburg C, Aberdam D, Shalom-Feuerstein R. SOX2 Regulates P63 and Stem/Progenitor Cell State in the Corneal Epithelium. Stem Cells 2019; 37:417-29. [PMID: 30548157].

11. Park JK, Yang W, Katsnelson J, Lavker RM, Peng H. MicroRNAs Enhance Keratinocyte Proliferative Capacity in a Stem Cell-Enriched Epithelium. PLoS One 2015; 10:e0134853-[PMID: 26248284].

12. Krol J, Loedige I, Filipowicz W. The widespread regulation of microRNA biogenesis, function and decay. Nat Rev Genet 2010; 11:597-610. [PMID: 20661255].

13. Dodsworth BT, Hatje K, Rostovskaya M, Flynn R, Meyer CA, Cowley SA. Profiling of naïve and primed human pluripotent stem cells reveals state-associated miRNAs. Sci Rep 2020; 10:10542-[PMID: 32601281].

14. Arpitha P, Prajna NV, Srinivasan M, Muthukkaruppan V. A method to isolate human limbal basal cells enriched for a subset of epithelial cells with a large nucleus/cytoplasm ratio expressing high levels of p63. Microsc Res Tech 2008; 71:469-76. d.[PMID: 18300290].

15. Arpitha P, Prajna NV, Srinivasan M, Muthukkaruppan V. A subset of human limbal epithelial cells with greater nucleus-to-cytoplasm ratio expressing high levels of p63 possesses slow-cycling property. Cornea 2008; 27:1164-70. [PMID: 19034133].

16. Kasinathan JR, Namperumalsamy VP, Veerappan M, Chidambaranathan GP. A novel method for a high enrichment of human corneal epithelial stem cells for genomic analysis. Microsc Res Tech 2016; 79:1165-72. [PMID: 27862636].

17. Kalaimani L, Devarajan B, Subramanian U, Ayyasamy V, Namperumalsamy VP, Veerappan M, Chidambaranathan GP. MicroRNA Profiling of Highly Enriched Human Corneal Epithelial Stem Cells by Small RNA Sequencing. Sci Rep 2020; 10:7418-[PMID: 32366885].

18. Ou H, Teng H, Qin Y, Luo X, Yang P, Zhang W, Chen W, Lv D, Tang H. Extracellular vesicles derived from microRNA-150–5p-overexpressing mesenchymal stem cells protect rat hearts against ischemia/reperfusion. Aging (Albany NY) 2020; 12:12669-83. [PMID: 32657760].

19. Wang DT, Ma ZL, Li YL, Wang YQ, Zhao BT, Wei JL, Qi X, Zhao XT, Jin YX. miR-150, p53 protein and relevant miRNAs consist of a regulatory network in NSCLC tumorigenesis. Oncol Rep 2013; 30:492-8. [PMID: 23670238].

20. Moles R, Bellon M, Nicot C. STAT1: A Novel Target of miR-150 and miR-223 Is Involved in the Proliferation of HTLV-I-Transformed and ATL Cells. Neoplasia 2015; 17:449-62. [PMID: 26025667].

21. Ghisi M, Corradin A, Basso K, Frasson C, Serafin V, Mukherjee S, Mussolin L, Ruggero K, Bonanno L, Guffanti A, De Bellis G, Gerosa G, Stellin G, D'Agostino DM, Basso G, Bronte V, Indraccolo S, Amadori A, Zanovello P. Modulation of microRNA expression in human T-cell development: targeting of NOTCH3 by miR-150. Blood 2011; 117:7053-62. [PMID: 21551231].

22. Tung CH, Kuo LW, Huang MF, Wu YY, Tsai YT, Wu JE, Hsu KF, Chen YL, Hong TM. MicroRNA-150–5p promotes cell motility by inhibiting c-Myb-mediated Slug suppression and is a prognostic biomarker for recurrent ovarian cancer. Oncogene 2020; 39:862-76. [PMID: 31570789].

23. Dai FQ, Li CR, Fan XQ, Tan L, Wang RT, Jin H. miR-150–5p Inhibits Non-Small-Cell Lung Cancer Metastasis and Recurrence by Targeting HMGA2 and β-Catenin Signaling. Mol Ther Nucleic Acids 2019; 16:675-85. [PMID: 31121479].

24. Sun JD, Li XM, Liu JL, Li J, Zhou H. Effects of miR-150–5p on cerebral infarction rats by regulating the Wnt signaling pathway via p53. Eur Rev Med Pharmacol Sci 2020; 24:3882-91. [PMID: 32329863].

25. Levis HJ, Kureshi AK, Massie I, Morgan L, Vernon AJ, Daniels JT. Tissue Engineering the Cornea: The Evolution of RAFT. J Funct Biomater 2015; 6:50-65. [PMID: 25809689].

26. Massie I, Kureshi AK, Schrader S, Shortt AJ, Daniels JT. Optimization of optical and mechanical properties of real architecture for 3-dimensional tissue equivalents: Towards treatment of limbal epithelial stem cell deficiency. Acta Biomater 2015; 24:241-50. [PMID: 26092352].

27. Sticht C, De La Torre C, Parveen A, Gretz N. miRWalk: An online resource for prediction of microRNA binding sites. PLoS One 2018; 13:e0206239-[PMID: 30335862].

28. Tokar T, Pastrello C, Rossos AEM, Abovsky M, Hauschild AC, Tsay M, Lu R, Jurisica I. mirDIP 4.1-integrative database of human microRNA target predictions. Nucleic Acids Res 2018; 46:D360-70. [PMID: 29194489].

29. Arpitha P, Prajna NV, Srinivasan M, Muthukkaruppan V. High expression of p63 combined with a large N/C ratio defines a subset of human limbal epithelial cells: implications on epithelial stem cells. Invest Ophthalmol Vis Sci 2005; 46:3631-6. [PMID: 16186343].

30. Kureshi AK, Dziasko M, Funderburgh JL, Daniels JT. Human corneal stromal stem cells support limbal epithelial cells cultured on RAFT tissue equivalents. Sci Rep 2015; 5:16186-[PMID: 26531048].

31. Levis HJ, Daniels JT. Recreating the Human Limbal Epithelial Stem Cell Niche with Bioengineered Limbal Crypts. Curr Eye Res 2016; 41:1153-60. [PMID: 26727236].

32. Barrandon Y, Green H. Three clonal types of keratinocyte with different capacities for multiplication. Proc Natl Acad Sci USA 1987; 84:2302-6. [PMID: 2436229].

33. Kanehisa M, Furumichi M, Sato Y, Ishiguro-Watanabe M, Tanabe M. KEGG: integrating viruses and cellular organisms. Nucleic Acids Res 2021; 49:D1D545-51. [PMID: 33125081].

34. Barbu MG, Condrat CE, Thompson DC, Bugnar OL, Cretoiu D, Toader OD, Suciu N, Voinea SC. MicroRNA Involvement in Signaling Pathways During Viral Infection. Front Cell Dev Biol 2020; 8:143-[PMID: 32211411].

35. Ran X, Xiao CH, Xiang GM, Ran XZ. Regulation of Embryonic Stem Cell Self-Renewal and Differentiation by MicroRNAs. Cell Reprogram 2017; 19:150-8. [PMID: 28277752].

36. Zhang J, Luo N, Luo Y, Peng Z, Zhang T, Li S. microRNA-150 inhibits human CD133-positive liver cancer stem cells through negative regulation of the transcription factor c-Myb. Int J Oncol 2012; 40:747-56. [PMID: 22025269].

37. Tian W, Zhu W, Jiang J. miR-150–5p suppresses the stem cell-like characteristics of glioma cells by targeting the Wnt/β-catenin signaling pathway. Cell Biol Int 2020; 44:1156-67. [PMID: 32009256].

38. Jung YS, Park JI. Wnt signaling in cancer: therapeutic targeting of Wnt signaling beyond β-catenin and the destruction complex. Exp Mol Med 2020; 52:183-91. [PMID: 32037398].

39. Lee SKW, Teng Y, Wong HK, Ng TK, Huang L, Lei P, Choy KW, Liu Y, Zhang M, Lam DS, Yam GH, Pang CP. MicroRNA-145 regulates human corneal epithelial differentiation. PLoS One 2011; 6:e21249-[PMID: 21701675].

40. Teng Y, Wong HK, Jhanji V, Chen JH, Young AL, Zhang M, Choy KW, Mehta JS, Pang CP, Yam GH. Signature microRNAs in human cornea limbal epithelium. Funct Integr Genomics 2015; 15:277-94. [PMID: 25487418].

41. Xu Z, Robitaille AM, Berndt JD, Davidson KC, Fischer KA, Mathieu J, Potter JC, Ruohola-Baker H, Moon RT. Wnt/β-catenin signaling promotes self-renewal and inhibits the primed state transition in naïve human embryonic stem cells. Proc Natl Acad Sci USA 2016; 113:E6382-90. [PMID: 27698112].

42. Davidson KC, Adams AM, Goodson JM, McDonald CE, Potter JC, Berndt JD, Biechele TL, Taylor RJ, Moon RT. Wnt/β-catenin signaling promotes differentiation, not self-renewal, of human embryonic stem cells and is repressed by Oct4. Proc Natl Acad Sci USA 2012; 109:4485-90. [PMID: 22392999].

43. Lee HJ, Wolosin JM, Chung SH. Divergent effects of Wnt/β-catenin signaling modifiers on the preservation of human limbal epithelial progenitors according to culture condition. Sci Rep 2017; 7:15241-[PMID: 29127331].

44. Luis TC, Naber BAE, Roozen PPC, Brugman MH, de Haas EF, Ghazvini M, Fibbe WE, van Dongen JJ, Fodde R, Staal FJ. Canonical wnt signaling regulates hematopoiesis in a dosage-dependent fashion. Cell Stem Cell 2011; 9:345-56. [PMID: 21982234].

45. González S, Oh D, Baclagon ER, Zheng JJ, Deng SX. Wnt Signaling Is Required for the Maintenance of Human Limbal Stem/Progenitor Cells In Vitro. Invest Ophthalmol Vis Sci 2019; 60:107-12. [PMID: 30640975].

46. He Z, Dang J, Song A, Cui X, Ma Z, Zhang Y. The involvement of miR-150/β-catenin axis in colorectal cancer progression. Biomed Pharmacother 2020; 121:109495-do.[PMID: 31731194].

47. MacDonald BT, Tamai K, He X. Wnt/beta-catenin signaling: components, mechanisms, and diseases. Dev Cell 2009; 17:9-26. [PMID: 19619488].

48. Wu SJ, Chen J, Wu B, Wang YJ, Guo KY. MicroRNA-150 enhances radiosensitivity by inhibiting the AKT pathway in NK/T cell lymphoma. J Exp Clin Cancer Res 2018; 37:18-[PMID: 29386059].

49. Zhang J, Shemezis JR, McQuinn ER, Wang J, Sverdlov M, Chenn A. AKT activation by N-cadherin regulates beta-catenin signaling and neuronal differentiation during cortical development. Neural Dev 2013; 8:7-[PMID: 23618343].

50. Workman A, Zhu L, Keel BN, Smith TPL, Jones C. The Wnt Signaling Pathway Is Differentially Expressed during the Bovine Herpesvirus 1 Latency-Reactivation Cycle: Evidence That Two Protein Kinases Associated with Neuronal Survival, Akt3 and BMPR2, Are Expressed at Higher Levels during Latency. J Virol 2018; 92:e01937-17. [PMID: 29321317].

51. Tian Q, Feetham MC, Tao WA, He XC, Li L, Aebersold R, Hood L. Proteomic analysis identifies that 14–3-3zeta interacts with beta-catenin and facilitates its activation by Akt. Proc Natl Acad Sci USA 2004; 101:15370-5. [PMID: 15492215].

52. Fang D, Hawke D, Zheng Y, Xia Y, Meisenhelder J, Nika H, Mills GB, Kobayashi R, Hunter T, Lu Z. Phosphorylation of beta-catenin by AKT promotes beta-catenin transcriptional activity. J Biol Chem 2007; 282:11221-9. [PMID: 17287208].

53. Sharma M, Chuang WW, Sun Z. Phosphatidylinositol 3-kinase/Akt stimulates androgen pathway through GSK3beta inhibition and nuclear beta-catenin accumulation. J Biol Chem 2002; 277:30935-41. [PMID: 12063252].

54. Baryawno N, Sveinbjörnsson B, Eksborg S, Chen CS, Kogner P, Johnsen JI. Small-molecule inhibitors of phosphatidylinositol 3-kinase/Akt signaling inhibit Wnt/beta-catenin pathway cross-talk and suppress medulloblastoma growth. Cancer Res 2010; 70:266-76. [PMID: 20028853].

55. Yang K, Wang X, Zhang H, Wang Z, Nan G, Li Y, Zhang F, Mohammed MK, Haydon RC, Luu HH, Bi Y, He TC. The evolving roles of canonical WNT signaling in stem cells and tumorigenesis: implications in targeted cancer therapies. Lab Invest 2016; 96:116-36. [PMID: 26618721].

56. Adhikari A, Davie J. JARID2 and the PRC2 complex regulate skeletal muscle differentiation through regulation of canonical Wnt signaling. Epigenetics Chromatin 2018; 11:46-[PMID: 30119689].

57. Steinhart Z, Angers S. Wnt signaling in development and tissue homeostasis. Development 2018; 145:dev146589-[PMID: 29884654].

58. Ghosh N, Hossain U, Mandal A, Sil PC. The Wnt signaling pathway: a potential therapeutic target against cancer. Ann N Y Acad Sci 2019; 1443:54-74. [PMID: 31017675].

Articles are provided courtesy of Emory University and the Zhongshan Ophthalmic Center, Sun Yat-sen University, P.R. China. The print version of this article was created on 7 August 2022. This reflects all typographical corrections and errata to the article through that date. Details of any changes may be found in the online version of the article.